LETTER

# Landau resonant modification of multiple kink mode contributions to 3D tokamak equilibria

IOP Publishing | International Atomic Energy Agency Nuclear Fusion

Nucl. Fusion **56** (2016) 014003 (5pp) doi:10.1088/0029-5515/56/1/014003

Letter

# Landau resonant modification of multiple kink mode contributions to 3D tokamak equilibria

**J.D. King[1], E.J. Strait[1], N.M. Ferraro[1], J.M. Hanson[2], S.R. Haskey[3], M.J. Lanctot[1], Y.Q. Liu[4], N.Logan[5], C. Paz-Soldan[1], D. Shiraki[6] and A.D. Turnbull[1]**

[1] General Atomics, San Diego, CA, USA
[2] Columbia University, New York, NY 10027, USA
[3] Plasma Research Laboratory, Research School of Physical Sciences and Engineering, The Australia National University, Canberra, ACT 0200, Australia
[4] Culham Centre for Fusion Energy, Culham Science Centre, Abingdon, Oxfordshire, OX14 3DB, UK
[5] Princeton Plasma Physics Laboratory, Princeton, NJ 08540, USA
[6] Oak Ridge National Laboratory, Oak Ridge, TN 37831, USA

E-mail: josh.king@science.doe.gov

Received 17 September 2015, revised 6 November 2015
Accepted for publication 23 November 2015
Published 17 December 2015

**Abstract**

Detailed measurements of the plasma's response to applied magnetic perturbations provide experimental evidence that the form of three-dimensional (3D) tokamak equilibria, with toroidal mode number $n = 1$, is determined by multiple stable kink modes at high-pressure. For pressures greater than the ideal magnetohydrodynamic (MHD) stability limit, as calculated without a stabilizing wall, the 3D structure transitions in a way that is qualitatively predicted by an extended MHD model that includes kinetic wave-particle interactions. These changes in poloidal mode structure are correlated with the proximity of rotation profiles to thermal ion bounce and the precession drift frequencies suggesting that these kinetic resonances are modifying the relative amplitudes of the stable modes. These results imply that each kink may eventually be independently controlled.

Keywords: tokamaks, equilibrium, magnetohydrodynamics, kinks, kinetic effects

(Some figures may appear in colour only in the online journal)

The application of 3D magnetic perturbations to tokamak plasmas may provide an ultimate means of maintaining stability and control of future fusion power plants. Instabilities like the edge localized mode [1] (ELM) and resistive wall mode [2] (RWM) are stabilized using applied 3D fields. Recently, the list of beneficial effects associated with these slight toroidal asymmetries has grown to include stabilizing torque injection [3] and a proof-of-principle demonstration of plasma burn control [4].

Conventionally, perturbations with toroidal mode number $n = 1$ were thought to be detrimental to stability, and much work has focused on their elimination, while edge localized $n > 1$ fields have been used to maintain ELM stability. However, recent DIII-D experiments show $n = 1$ fields play a critical role in suppressing ELMs [5, 6]. For practical reasons, fusion power plants will favor locating 3D coils at large major radius (outside of blanket materials). Hence, designing a 3D plasma equilibrium that is core-to-edge stable using deeply penetrative low $n$ fields is desirable.

3D equilibria are often assumed to be dominated by a single marginally stable eigenmode that depends on the stability

 

properties of the 2D equilibrium and not the structure of the applied external field [7]. However, results from the HBT-EP tokamak clearly identified the co-existence of multiple current driven kink modes [8, 9]. Furthermore, observations of 'non-rigid' RWM growth [2] suggest that multiple modes may also be important at high-pressure. For clarity, we will refer to the *stable* RWM [10, 11], which is an ideal kink *instability* with growth rate (when unstable) defined by the resistive timescale of a nearby conducting wall, as a 3D equilibrium. It is important to note, mathematically the structure of a single kink mode, in a strongly shaped, finite aspect ratio tokamak, can be described by a set of many linearly coupled poloidal harmonics ($m$ numbers). Here multiple distinct eigenmodes of the system are discussed, each of which can be represented by the same basis set of poloidal harmonics. Furthermore, helicity variations of these tokamak discharges are such that a more internal global kink eigenmode will be dominated by smaller $m$ components, while the opposite is true for the more external kinks.

At high pressure, kinetic wave-particle interactions (ion Landau damping) have been identified as a passive stabilization mechanism for preventing RWM growth [10–13], but a connection between mode stability and structure has remained elusive. 3D equilibria for discharges with rapid toroidal rotation were theorized to result from RWM energy loss to trapped particle banana transits [14] (bounces). But the experimental observation of RWM stability at slow rotation required the extension of this theory to include trapped particle precession drifts [15]. Measurements in DIII-D found a signature trend in the amplitude of 3D equilibria, which is peaked when the plasma rotation profile is away from both fast and slow thermal particle resonances [10].

In this Letter, we present experimental evidence and modeling showing multiple stable $n = 1$ kink modes are present in a single tokamak 3D equilibrium. Changes in the relative stability of the modes are correlated with radial differences in trapped thermal particle damping, and appear to cause the 3D structure to vary at high pressure, unifying these previously disparate observations.

In these DIII-D experiments, stable kink mode perturbations are stimulated in weakly shaped, H-mode discharges. The perturbations are applied using 2 toroidal arrays of 6 equidistant, picture frame, active coils. The arrays are located above and below the midplane. A constant amplitude $n = 1$ field is applied and rotated at 10 Hz. The toroidal phase difference between the upper and lower I-coils ($\Delta\phi_{\rm UL}$) is maintained constant during rotation. Changes in the $\Delta\phi_{\rm UL}$ modify the poloidal spectrum for a single $n$. The plasma's response to this field is measured synchronously using dedicated magnetic sensor pairs [16]. The main toroidal array of sensors is capable of resolving toroidal mode numbers $n \leqslant 3$, but in this experiment the measured plasma response with $n > 1$ is negligible. We consider the vertical component of the field measured along the height of the high field side (HFS) wall. Using a toroidal field of $B_0 = 1.8$ T and a plasma current of $I_{\rm P} = 1.2$ MA, we obtain a safety factor at the 95% poloidal flux surface $q_{95} \sim 4.3$. The toroidal rotation profiles are varied via a neutral beam injected (NBI) torque scan ($T_{\rm NBI} = 2.0, 4.0, 6.0$, and 8.0 N m) while maintaining constant beta (the ratio of plasma to magnetic pressure). This is accomplished by changing the portion of NBI directed in the co and counter $I_{\rm P}$ direction, while maintaining constant injected power. The normalized beta is maintained above the no-wall limit ($\beta_{\rm N}^{\rm no\text{-}wall}$), which is the ideal MHD stability limit assuming no nearby conducting boundary is present. This limit is readily exceeded in DIII-D [17]. For the axisymmetric equilibria considered here, the ideal MHD no-wall limit calculated with DCON [18] has normalized beta $\beta_{\rm N} \sim 2.2$, where $\beta_{\rm N} = \beta(aB/I_{\rm P})$ and $a$ is the plasma minor radius.

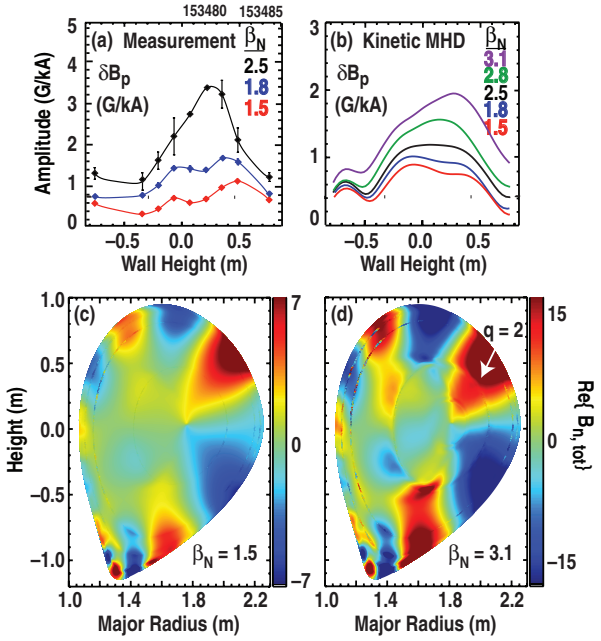


**Figure 1.** Pressure variation of the ($a$) measured and ($b$) kinetic MHD predicted plasma response vertical field amplitude along the HFS wall. The kinetic MHD theoretical prediction of the normal field response throughout the plasma volume ($c$) below and ($d$) above $\beta_N^{\rm no\text{-}wall}$, where inside $q = 2$ an additional internal kink contributes.

To first determine if kinetic effects impact the 3D structure, measurements of the plasma response are obtained above and below the $\beta_N^{\rm no\text{-}wall}$ (figure 1($a$)). Both model and measurement show a distinct change in the response at high pressure. Shown in figure 1($a$) are the measured response amplitude profiles along the HFS of DIII-D for three values of $\beta_{\rm N}$. These profiles have constant applied fields, yet the mode structure changes qualitatively, suggesting a new 3D equilibrium is reached when $\beta_{\rm N} > \beta_N^{\rm no\text{-}wall}$. Below $\beta_N^{\rm no\text{-}wall}$ the response nearly scales by a constant multiplier, which is consistent with previous measurements and modeling [19–22]. Two local maxima located at $Z = -0.1$ m and $Z = +0.4$ m assume a new state at $\beta_{\rm N} = 2.5$ with a single maximum value peaked at $Z = +0.3$ m. Kinetic MHD model results (MARS-K [23, 24]), shown in figure 1($b$), exhibit a similar transition, albeit at higher pressures. Here $\beta_{\rm N}$ is scaled between 1.5 and 3.1.

The similarity of the $\beta_{\rm N} = 3.1$ predicted (figure 1($b$)) and $\beta_{\rm N} = 2.5$ experimental (figure 1($a$)) external plasma response profiles suggest that the physical equations solved within

this model are sufficient to describe the qualitative behavior of the plasma within this regime. However, more work is needed to resolve the difference in the onset pressure for this structural transition, the quantitative difference in the average amplitudes, and the difference in the vertical location of the dominant response peak for the lower beta cases. Included in this self-consistent computation of the kinetic pressure tensor are passing particle resonances, as well as trapped particle bounce and precession resonances. In all cases the total modeled change in potential energy, including these kinetic terms, is positive ($\delta W > 0$), such that only externally driven 3D equilibria are computed.

These kinetic MHD predictions provide indirect evidence of an additional kink contribution originating in the plasma core for $\beta_N > \beta_N^{\text{no-wall}}$. External magnetic measurements alone are insufficient to directly determine the internal 3D equilibria. However, with sufficiently detailed agreement of the predicted external response, the internal response may be inferred. Contours of the predicted total response normal to the unperturbed flux surfaces at a single toroidal angle are shown in figures 1(*c*) and (*d*). Below $\beta_N^{\text{no-wall}}$ (figure 1(*c*)) a single distinct kink structure is apparent throughout the plasma volume. For the $\beta_N = 3.1$ case (figure 1(*d*)) significant differences near and inside the $q = 2$ surface are apparent. The contour distortions on either side of this rational surface are due to an additional core kink mode.

Measurements (figure 1(*a*)) show the response to be non-rigid, and modeling (figures 1(*b*)–(*d*)) suggests this non-rigidity is due to multiple kink contributions. To definitively determine if multiple modes contribute to the response, the $\Delta\phi_{\text{UL}}$ is varied. For a single-mode description, changing the coupling ($\Delta\phi_{\text{UL}}$), drive ($\beta_N$), or damping (rotation) should only change the amplitude of the kink mode. Figure 2(*a*) shows that a single-mode description holds for all conditions except $\beta_N = 2.5$, and $\Delta\phi_{\text{UL}} = 240°$. Here the amplitude is normalized to the average amplitude for each profile. The phase profiles of all cases are consistent with a helical kink structure (not all phase data is shown for clarity). For $\beta_N = 2.5$, the structure of the mode qualitatively deviates only when the applied poloidal content of the field ($\Delta\phi_{\text{UL}}$) is modified. This shows that multiple kink modes are contributing to the plasma response.

To radially localize the wave-particle interactions with these multiple kink modes, we modify the internal plasma rotation profiles at constant beta. Figure 3 shows the 2D equilibrium $q$ and total pressure profiles for the discharges considered. These profiles are comparable, although for the $T_{\text{NBI}} = 8\,\text{N m}$ case $q_{95} \sim 4.2$, while for the lower torque cases $q_{95} \sim 4.5$. Figure 3(*b*) shows the measured plasma rotation profiles, and approximations of the trapped thermal particle resonant frequencies. Here we consider the rotation due to the radial electric field $\omega_E \equiv -\text{d}\phi/\text{d}\psi$, where $\phi$ is the electrostatic potential and $\psi$ is the poloidal flux. This rotation incorporates measurements of both the toroidal and poloidal components of the rotation. The thermal ion bounce and the precession drift frequencies are estimated using the same expressions as in [10], $\omega_b \approx [r/(2R)]^{0.5}\, V_{i,th}/(qR)$ and $\langle\omega_D\rangle_b \approx qV_{i,th}^2/(\omega_{ci} rR)$,

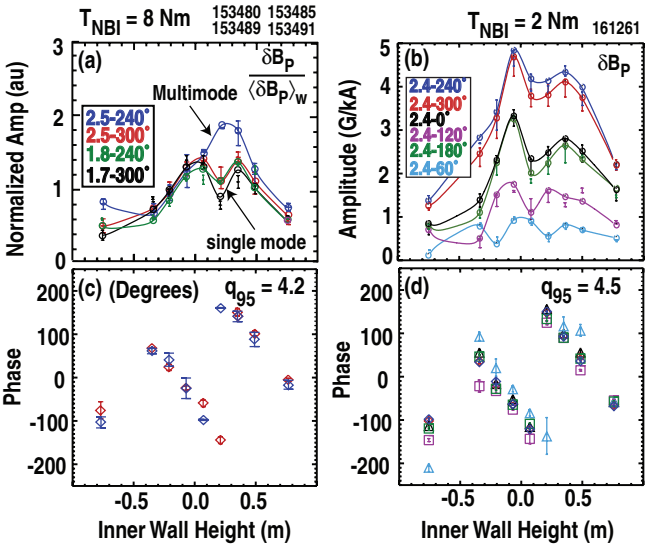


**Figure 2.** HFS plasma response measurements (vertical bars), SVD reconstruction (circle), spline fit to SVD reconstruction (curves) and phase data (diamonds) with (*a*) normalized amplitude for $\beta_N$–$\Delta\phi_{\text{UL}}$: 2.5 – 240° (blue) exhibiting strong multimode response, 2.5–300° (red), 1.8–240° (green), and 1.7–300° (black), with $T_{\text{NBI}} = 8\,\text{N m}$, and (*b*) amplitude (G kA$^{-1}$) for $T_{\text{NBI}} = 2\,\text{N m}$, $\beta_N = 2.4$ and $\Delta\phi_{\text{UL}}$: 240° (blue), 300° (red), 0° (black), 60° (cyan), 120° (purple), and 180° (green). Phase (degrees) are shown in (*c*) and (*d*).

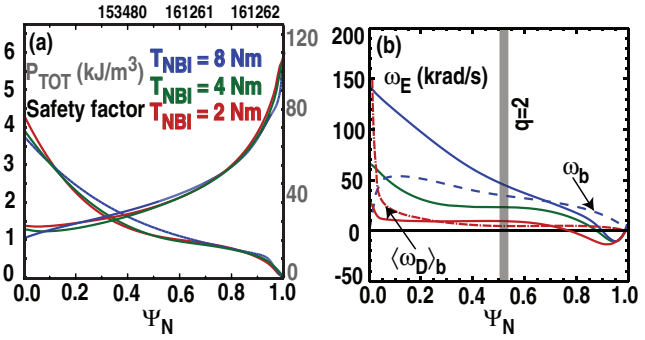


**Figure 3.** For $T_{\text{NBI}} = 2$ (red), 4 (green), and 8 N m (blue), the experimental (*a*) safety factor and pressure profiles (kJ m$^{-3}$), as well as (*b*) rotation (krad s$^{-1}$) profiles are shown. Also approximations of the precession drift resonant frequency (dash–dotted line) and bounce frequency (dashed line).

where $V_{i,th}$ is the ion thermal velocity, $R$ is major radius, $r$ the minor radius, $\omega_{ci}$ the ion cyclotron frequency, $\langle\rangle_b$ denotes bounce averaging. This approximation does not include information about the exact particle energies and the pitch angles of the particles with respect to the wave being damped. Despite these finer details a key observation becomes apparent, the proximity of the rotation profile to the resonant frequencies should give rise to differences in the damping across the plasma volume, allowing changes in the relative stability for multiple modes. For $T_{\text{NBI}} = 8\,\text{Nm}$, $\omega_E$ is near the bounce frequency outside the $q = 2$ surface. At deeper radius the frequencies diverge. This would be expected to cause weak damping in the plasma core (inside $q = 2$) and stronger damping near the edge, changing the relative stability of each mode such that an additional kink (inside $q = 2$) contributes to the

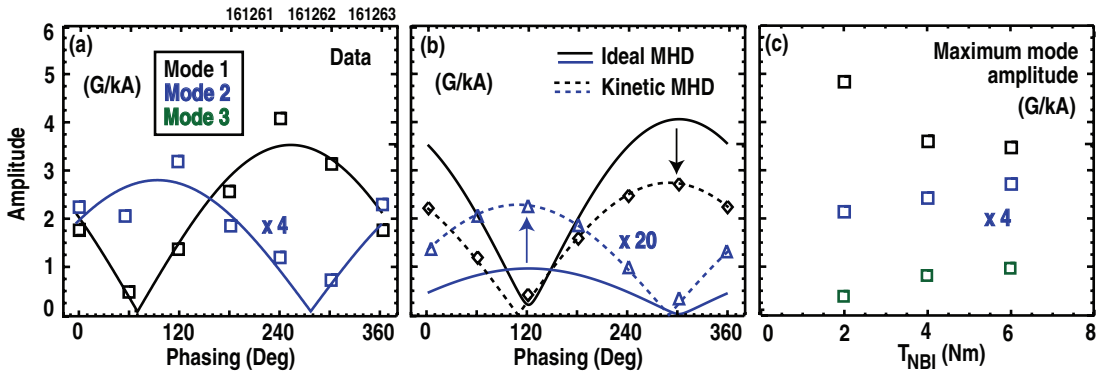


**Figure 4.** Multimode plasma response measurements of (*a*) experimental vector amplitudes (G kA$^{-1}$) from SVD fits to the a $T_{\mathrm{NBI}} = 6$ N m discharge 161263 showing a dominant mode (mode 1) and a secondary mode (mode 2) $\Delta\phi_{\mathrm{UL}}$ dependence, (*b*) ideal (solid line) and kinetic (diamond and triangle symbols) MHD modeled amplitudes (G/kA) for SVD fits of the plasma response showing a similar $\Delta\phi_{\mathrm{UL}}$ dependence for both modes, (*c*) The peak amplitude for each mode measured for $T_{\mathrm{NBI}} = 2$, 4, and 6 N m, including an additional mode (mode 3).

external response (figures 1(*a*) and 2(*a*)). This is consistent with the previous kinetic modeling that shows an additional kink mode contribution inside $q = 2$ for this same discharge (figure 1(*d*)).

When $\omega_{\mathrm{E}}$ is well aligned with a kinetic resonance across the entire minor radius (figure 3(*b*)—$T_{\mathrm{NBI}} = 2$ N m), the response appears to return to that expected for a single-mode. Figure 2(*b*) shows the HFS plasma response for a $\Delta\phi_{\mathrm{UL}}$ scan for $T_{\mathrm{NBI}} = 2$ Nm. All data in this panel has $\beta_{\mathrm{N}} > \beta_N^{\text{no-wall}}$. In figure 3(*b*), $\omega_{\mathrm{E}}$ of the $T_{\mathrm{NBI}} = 2$ Nm case aligns with $\langle\omega_{\mathrm{D}}\rangle_{\mathrm{b}}$ for nearly the entire plasma volume. The transition seen for the $T_{\mathrm{NBI}} = 8$ Nm case at $\Delta\phi_{\mathrm{UL}} = 240°$ (figure 2(*a*)), indicating the presence of multiple modes, is no longer apparent. The amplitude (figure 2(*b*)) and phase (figure 2(*d*)) show a largely invariant shape for all $\Delta\phi_{\mathrm{UL}}$ except those that are least coupled to the external kink (60° and 120°). However, for the 3D equilibrium to consist of only a single dominant mode the response amplitude must scale for every $\Delta\phi_{\mathrm{UL}}$. The deviation of any response profile beyond the measurement uncertainty implies multiple modes are still contributing.

If we assume that each sensor measurement represents the superposition of several stable plasma modes having different spatial structures and different dependences on $\Delta\phi_{\mathrm{UL}}$, then these modes can be separated using singular value decomposition (SVD). A 2D matrix $\boldsymbol{M}_{ij}$ of measurements versus nine sensor positions $Z$ (indexed by $j$) and six differential coil phasings $\Delta\phi_{\mathrm{UL}}$ (indexed by $i$) is obtained from time series analysis of each case ($i$,$j$), where each matrix element is a complex number representing the amplitude and phase shift of the plasma response relative to the applied field. SVD analysis is then used to decompose the measurement matrix as $M_{ij} = \sum_k \lambda_k F_k(Z_j) G_k(\Delta\phi_i)$, where the $F_k$ and $G_k$ are sets of orthonormal functions of the sensor position and the form of the applied field, respectively. For the $\boldsymbol{T}_{\mathrm{NBI}} = 2$, 4, and 6 N m cases, retaining only the one SVD eigenmode with the largest singular value $\lambda_k$ does not reconstruct the data. Instead, the two or three SVD modes with largest weights must be retained in order to reconstruct the measurements to within the experimental uncertainty; this result strongly suggests that the measured response is determined by several independent plasma modes. The circles shown in the amplitude profiles in figure 2 correspond to these reconstructed values and closely match the data.

The hypothesis that the SVD eigenmodes indeed correspond to multiple plasma modes is supported by $\Delta\phi_{\mathrm{UL}}$—response trends. The peak amplitudes corresponding to the first two eigenmodes are plotted versus $\Delta\phi_{\mathrm{UL}}$ in figure 4(*a*) for the 6 N m case. As shown by the solid curves, each set of amplitudes agrees well with the function $A(\Delta\phi_{\mathrm{UL}}) \propto \left|\cos((\Delta\phi_{\mathrm{UL}} - \Delta\phi_0)/2)\right|$. This dependence is expected for coupling to a helical plasma mode. When the $\Delta\phi_{\mathrm{UL}}$ is aligned with the helicity of the mode ($\Delta\phi_{\mathrm{UL}} = \Delta\phi_0$), the coupling is strongest and the amplitude of the mode will be peaked. For misaligned differential phasings ($\Delta\phi_{\mathrm{UL}} \neq \Delta\phi_0$) the mode is driven to a toroidal location midway between the peak fields of the upper and lower coils. Restated, the peak at $\Delta\phi_{\mathrm{UL}} = \Delta\phi_0$ corresponds to the coil differential phasing with maximum coupling (e.g. mode 1 at $\Delta\phi_{\mathrm{UL}} = 240°$), while the null, 180° away, corresponds to an 'orthogonal' field configuration with no coupling to that specific plasma mode. In figure 4(*b*), identical SVD analysis is carried out for the modeled response. For the ideal calculation, the linearity of the MARS-F code allows for arbitrarily small resolution in $\Delta\phi_{\mathrm{UL}}$ without additional computation [25, 26]. It is important to note that no plasma physics is included in this SVD analysis, yet the qualitative $\Delta\phi_{\mathrm{UL}}$ trends are consistent with multiple plasma modes predicted by the MARS-F/K codes.

Previous measurements and modeling have shown that the low field side helicity of an external kink with $q_{95}$ ~ 4 ($q_{95}$ ~ 3) is aligned with a $\Delta\phi_{\mathrm{UL}}$ of 300° (240°), resulting in the strongest mode coupling [27]. Based on this rough metric, we hypothesize that each mode's peak response should be associated with a unique $\Delta\phi_{\mathrm{UL}}$ and that a deeper core mode (near the $q = 2$ rational surface) should peak for more pitched $\Delta\phi_{\mathrm{UL}}$ (<240°). The dominant external kink mode (mode 1) has a peak response amplitude for a lesser pitched differential phasing ($\Delta\phi_{\mathrm{UL}}$ ~ 300°), while the secondary mode (mode 2) is peaked at a greater pitched applied field ($\Delta\phi_{\mathrm{UL}}$ ~ 140°), which is consistent with expectations of a core mode originating near the $q = 2$ surface.

Because the externally measured response profiles are due to a combination of the kink modes, the relative contribution of the core mode to the external response is clearest when the dominant mode (at greater radius) is weakly coupled ($\Delta\phi_{UL} = 60°$ and 120°), hence the observable difference in the response profiles that is seen for these two cases (figure 2(*b*)).

Trends in the relative amplitudes of each mode are correlated to the proximity of the internal rotation and kinetic frequency profiles. The change in mode amplitudes is shown in figure 4(*c*), where data from a scan of 6 different $\Delta\phi_{UL}$'s, like that shown in figures 2(*b*) and (*d*), is analysed to determine the 3 mode amplitudes at each $T_{NBI}$. In all the cases, mode 1 peaks at $\Delta\phi_{UL} = 260° \pm 8°$ and the core mode (mode 2) peaks at $\Delta\phi_{UL} = 130° \pm 20°$. The amplitude of the dominant mode (mode 1) decreases and the amplitudes of the secondary (mode 2) and tertiary (mode 3) modes increase as $T_{NBI}$ increases. In comparing the 4 N m ($\omega_{E,g}$) and 2 N m ($\omega_{E,r}$) rotation profiles (figure 3(*b*)) for $0.8 < \psi_N < 0.95$, it can be seen that $\omega_{E,r} < \omega_{E,g} \sim \langle\omega_D\rangle_b$ suggesting stronger local kinetic damping is responsible for this decrease in the dominant mode response. Similarly, near $q = 2$ the $\omega_{E,r} \sim \langle\omega_D\rangle_b < \omega_{E,g} < \omega_b$ suggesting the damping near this radius should be less and that the corresponding mode amplitude should increase.

While modeling (figure 4(*b*)) does not quantitatively capture the measured response amplitude of the 2nd mode, the inclusion of kinetic effects qualitatively predicts a nonuniform impact on mode stability, consistent with experimental observation. Disagreement in the absolute amplitude of the 2nd mode may result from neglecting toroidal asymmetries in core neutral beam anisotropic energetic particle distributions, which recent theory has found to alter 3D stability [28]. The kinetic MHD predicted peak amplitudes for each mode are factors of 1.3 and 6.1 less than measurement for the 1st and 2nd mode, respectively. Measurements show the peak response amplitude of mode 2 is ~4.8 times smaller than mode 1. From figure 4(*b*), it is seen that the inclusion of kinetic damping does not impact the response uniformly, rather the amplitude of mode 2 increases by a factor of 2 and the amplitude of mode 1 decreases by a factor of 2 when compared to ideal predictions. This provides further evidence that kinetic effects may be responsible for the changes in the relative stability of multiple kink modes.

## Summary and discussion

Detailed measurements and modeling of $n = 1$ 3D equilibria provide the first highly suggestive evidence that trapped thermal particle resonances alter the relative stability of multiple kink modes above $\beta_N^{\text{no-wall}}$, providing a new avenue to improve externally applied nonaxisymmetric fields in tokamaks. Singular value decomposition analysis shows that trends in the amplitudes of each mode are consistent with a core kink contribution ($q \sim 2$) as well as the dominant kink for $q_{95} = 4.5$. The local proximity of radial rotation profiles to kinetic damping resonances is correlated with changes in the relative amplitude of multiple modes. For low $T_{NBI}$, the measured plasma rotation is comparable to that expected in a first burning plasma, and the response is dominated by a single mode, implying $n = 1$ error field correction may be insensitive to the non-axisymmetric coil geometry so long as there is some coupling to the mode.

The unique spatial character of each mode may eventually enable 3D field optimization, through the application of only an $n = 1$ field. Recent studies [6] suggest ELM suppression is partially caused by a driven $n = 1$ magnetic island response! Also, quiescent H-mode studies in DIII-D have identified nonlinear harmonic coupling with low-$n$ ($n = 1$, 2) modes as a mechanism for maintaining stationary ELM-free conditions [29]. We speculate that the stimulation or nulling of multiple kink eigenmodes and/or islands could allow $n = 1$ fields to be poloidally tailored to maintain plasma stability from core-to-edge in future devices.

## Acknowledgments

This material is based upon work supported by the US Department of Energy, Office of Science, Office of Fusion Energy Sciences, using the DIII-D National Fusion Facility, a DOE Office of Science user facility, under Awards DE-FC02-04ER54698, DE-FG02-04ER54761, DE-AC02-09CH11466, and DE-AC05-00OR23100. DIII-D data shown in this paper can be obtained in digital format by following the links at https://fusion.gat.com/global/D3D_DMP. The authors wish to thank Z. Wang and F. Turco for their MARS-F/K support.

## References

[1] Evans T.E. *et al* 2006 *Nat. Phys.* **2** 419
[2] Sabbagh S.A. *et al* 2006 *Phys. Rev. Lett.* **97** 045004
[3] Garofalo A.M. *et al* 2008 *Phys. Rev. Lett.* **101** 195005
[4] Hawryluk R.J. *et al* 2015 *Nucl. Fusion* **55** 053001
[5] Paz-Soldan C. *et al* 2015 *Phys. Rev. Lett.* **114** 105001
[6] Nazikian R. *et al* 2015 *Phys. Rev. Lett.* **114** 105002
[7] Boozer A.H. 2001 *Phys. Rev. Lett.* **86** 5059
[8] Maurer D.A. *et al* 2012 *Phys. Plasmas* **19** 056123
[9] Shiraki D. *et al* 2013 *Phys. Plasmas* **20** 102503
[10] Reimerdes H. *et al* 2011 *Phys. Rev. Lett.* **106** 215002
[11] Reimerdes H. *et al* 2007 *Phys. Rev. Lett.* **98** 055001
[12] Takechi M. *et al* 2007 *Phys. Rev. Lett.* **98** 055001
[13] Berkery J.W. *et al* 2010 *Phys. Plasmas* **17** 082504
[14] Bondeson A. and Chu M.S. 1996 *Phys. Plasmas* **3** 3013
[15] Hu B. and Betti R. 2004 *Phys. Rev. Lett.* **93** 105002
[16] King J.D. *et al* 2014 *Rev. Sci. Instrum.* **85** 083503
[17] Strait E.J. *et al* 1995 *Phys. Rev. Lett.* **74** 2418
[18] Glasser A.M. and Chance M.S. 1997 *Bull. Am. Phys. Soc.* **42** 1848
[19] Lanctot M.J. *et al* 2011 *Phys. Plasmas* **18** 056121
[20] Chapman I.T. *et al* 2014 *Nucl. Fusion* **54** 083006
[21] Chapman I.T. *et al* 2014 *Nucl. Fusion* **54** 083007
[22] King J.D. *et al* 2015 *Phys. Plasmas* **22** 072501
[23] Liu Y.Q. *et al* 2000 *Phys. Plasmas* **7** 3681
[24] Liu Y.Q. *et al* 2008 *Phys. Plasmas* **15** 112503
[25] Haskey S.R. *et al* 2014 *Plasma Phys. Control. Fusion* **56** 035005
[26] Haskey S.R. *et al* 2015 *Plasma Phys. Control. Fusion* **57** 025015
[27] Lanctot M.J. *et al Phys. Plasmas* **17** 030701
[28] Liu Y. *et al* 2010 *Phys. Plasmas* **21** 056105
[29] Liu F. *et al* 2015 *Nucl. Fusion* **55** 113002